Seasonality of Holocene hydroclimate in the Eastern Mediterranean reconstructed using the oxygen isotope composition of carbonates and diatoms from Lake Nar, central Turkey

Jonathan R Dean[1,2,3,4 *], Matthew D Jones[2,3], Melanie J Leng[1,3], Sarah E Metcalfe[2,3], Hilary J Sloane[1], Warren J Eastwood[5] and C Neil Roberts[6]

[1]*NERC Isotope Geosciences Facilities, British Geological Survey, UK*

[2]*School of Geography, University of Nottingham, UK*

[3]*Centre for Environmental Geochemistry, University of Nottingham, UK*

[4]*School of Environmental Sciences, University of Hull, UK*

[5]*School of Geography, Earth and Environmental Sciences, University of Birmingham, UK*

[6]*School of Geography, Earth and Environmental Sciences, University of Plymouth, UK*

*Corresponding author Jonathan R Dean

j.dean2@hull.ac.uk

School of Environmental Sciences, University of Hull, Hull HU6 7RX UK

Abstract

A positive shift in the oxygen isotope composition ($\delta^{18}O$) of lake carbonates in the Eastern Mediterranean from the early to late Holocene is usually interpreted as a change to drier (reduced P/E) conditions. However, it has also been suggested that changes in the seasonality of precipitation could explain these trends. Here, Holocene records of $\delta^{18}O$ from both carbonates and diatom silica, from Lake Nar in central Turkey, provide insights into palaeoseasonality. We show how $\Delta\delta^{18}O_{lakewater}$ (the difference between spring and summer reconstructed $\delta^{18}O_{lakewater}$) was minimal in the early Holocene and for most of the last millennium, but was greater at other times. For example, between ~4,100-1,600 years BP we suggest that increased $\Delta\delta^{18}O_{lakewater}$ could have been the result of relatively more spring/summer evaporation, amplified by a decline in lake level. In terms of change in annual mean $\delta^{18}O$, isotope mass balance modelling shows that this can be influenced by changes in seasonal P/E as well as inter-annual P/E, but lake level falls inferred from other proxies confirm there was a mid Holocene transition to drier climatic conditions in central Turkey.

Keywords

Oxygen isotopes; Eastern Mediterranean; lake sediment; Mid Holocene Transition; palaeoseasonality; Turkey

1 Introduction

Understanding the detail of hydrological variability over multiple timescales is important in regions such as the Eastern Mediterranean where water stress is increasing (Issar and Adar, 2010) and where management of water supplies under a changing climate is essential (e.g. Kelley et al., 2015). Water availability issues have potentially been critical for societies in the region for millennia (e.g. Weiss et al., 1993) and an understanding of both changes in mean state and seasonality are required (Rohling, 2016). Many studies from the region have shown a shift in the mid Holocene to higher oxygen isotope ratios of lake carbonates ($\delta^{18}O_{carbonate}$) (Roberts et al., 2008). These are usually interpreted as responding to changes in the balance between precipitation and evaporation (P/E) (Jones and Roberts, 2008), thus showing a mid Holocene transition from a wetter early Holocene, with relatively more precipitation, to a drier late Holocene, where evaporation losses were relatively increased. However, the extent to which there were shifts in the seasonality of precipitation in the Holocene, and the degree to which these would have affected $\delta^{18}O_{carbonate}$, remains an unresolved issue in Eastern Mediterranean Holocene palaeoclimatology. Stevens et al. (2001, 2006) suggested that a change from winter- to spring-dominated precipitation was potentially a driver of the increasing $\delta^{18}O_{carbonate}$ trend in the mid Holocene, based on analysis of the sediments of Lakes Zeribar and Mirabad in Iran. Other authors, using pollen and

microcharcoal records, have also argued that there were shifts in the seasonality of precipitation in the region through the Holocene (e.g. Djamali et al., 2010; Turner et al., 2010; Peyron et al., 2011).

Seasonality change analysis requires proxies that are sensitive to different seasons. Dean et al. (2013) showed that comparing $\delta^{18}O$ from endogenic carbonates and diatoms at Nar Gölü (Gölü = lake in Turkish) in central Anatolia can provide insights into seasonality as they formed/grew at different times of the year. Such records, combining $\delta^{18}O$ from diatoms and carbonates in the same core, remain rare. Here, we present a $\delta^{18}O_{carbonate}$ vs. $\delta^{18}O_{diatom}$ record from Nar Gölü for the entire Holocene, developing a rigorous methodology for diatom isotope data correction, coupled with an isotope mass balance model, to investigate how and why intra-annual variability (seasonality) of $\delta^{18}O_{lakewater}$ changed over time.

2 Site description and core material

Nar Gölü (38°20’24’’N, 34°27’23’’E; 1363 m.a.s.l.; Figure 1) is a maar lake, ~0.6 km^2 in area and >20 m deep, located in the Cappadocia region of central Turkey. The climate of the region is continental Mediterranean (Kutiel and Türkeş, 2005), with precipitation at a nearby meteorological station in Niğde, 45 km from Nar Gölü,

averaging 339 mm per year and peaking in April and May. The crater geology is dominated by basalt and ignimbrite (Gevrek and Kazancı, 2000). The limnology and contemporary sedimentation patterns are described in detail in Dean et al. (2015a), but in summary endogenic carbonate precipitation in the lake surface waters is weighted towards the early summer (end of June/beginning of July), whereas diatom production is weighted towards the spring (end of March/beginning of April). There was ~1.6‰ intra-annual variability in $\delta^{18}O_{lakewater}$ through our June 2011 to July 2012 monitoring period (the period for which we have samples through all seasons), ~0.5‰ of which occurred between the estimated time of peak diatom growth in spring 2012 and carbonate formation in the early summer 2012 (Figure 2). We believe the timing of diatom growth and carbonate precipitation is likely to have stayed roughly the same through the Holocene. As we show in section 4, $\delta^{18}O_{lakewater}$ reconstructed for the time of diatom growth is almost always lower than $\delta^{18}O_{lakewater}$ reconstructed for the time of carbonate precipitation, and this would not be the case if diatom growth was weighted to the summer or early autumn (Figure 2). Indeed, previous work showed there were three planktonic/facultative planktonic 'bloom' taxa common in the Nar Gölü diatom record over the last 1,700 years that are likely to have been spring blooming: *Synedra acus, Nitzschia palaeacea* and *Cyclotella meneghiniana* (Woodbridge and Roberts 2011). These taxa were also the dominant 'bloom' diatoms in the early Holocene (11,700-6,500 years BP) and it is reasonable to assume that their seasonal ecology was

the same at that time as during the late Holocene. The only additional early Holocene bloom diatom is *Aulacoseira ambigua*, but this is only important in two samples (11,657 and 11,403 years BP). In the section from 4,400-3,900 years BP it is possible that *Nitzschia palaea* was a bloom taxon and it is likely to have been spring blooming like *N. palaeacea*. The majority of carbonate is always likely to have precipitated in the early summer in response to increasing evaporation (Dean et al., 2015a).

Figure 1

Figure 2

There have been a number of previous palaeolimnological investigations of the Nar Gölü sediments (e.g. Jones et al., 2006; England et al., 2008; Woodbridge and Roberts, 2010). Here we combine data from the original core sequence taken in 2001/2 (NAR01/02) with new data from a longer core sequence taken in 2010 (Roberts et al., 2016). The chronology of the NAR10 core was constructed by combining varve counting and U-Th dates (Dean et al., 2015b).

3 Methods

120 *3.1 Isotope sample preparation and mass spectrometry*

121

122 $\delta^{18}O_{carbonate}$ data were produced using classic vacuum techniques and an Optima dual-
123 inlet mass spectrometer, as described in detail in Dean et al. (2015b). Specifically, the
124 carbonate analysed for isotopes from the Nar Gölü record was calcite and aragonite, as
125 detailed in Dean et al. (2015b). Data are given as ‰ deviations from VPDB and
126 analytical reproducibility was 0.1‰ for $\delta^{18}O$ and $\delta^{13}C$.

127

128 Samples for $\delta^{18}O_{diatom}$ analysis need to be as free as possible of non-diatom material
129 since the analytical methods used will liberate oxygen from these other components of
130 the sediment, such as carbonate and detrital silicates. Samples were therefore processed
131 using techniques similar to those of Morley et al. (2004), with the use of hydrogen
132 peroxide, nitric acid (to help remove organics; Tyler et al., 2007), hydrochloric acid,
133 differential settling, sieving at 10 μm and heavy liquid separation stages. $\delta^{18}O_{diatom}$
134 analysis was carried out on cleaned diatom samples using the stepwise fluorination
135 technique and a Thermo Finnigan MAT 253 at the NERC Isotope Geosciences
136 Facilities. The method is described in Leng and Sloane (2008) and has been verified
137 through an inter-laboratory comparison exercise (Chapligin et al., 2011). The data are
138 presented as ‰ deviations from VSMOW and analytical reproducibility was 0.3‰.

139

Diatom isotope samples prepared from ~8,800-7,900 and ~4,000-2,350 years BP had insufficient diatom silica for analysis, although there were still diatoms growing in the lake at this time (Roberts et al., 2016).

3.2 Correction of diatom isotope data

The samples from Nar Gölü still contained residual detrital silicates after the preparation described above due to a lack of density contrast between the detrital silicates and the diatoms, which reduced the efficacy of heavy liquid separation (Dean et al., 2013). A correction was, therefore, applied to account for the impact of detrital silicates on $\delta^{18}O$ (Mackay et al. 2011):

$$\delta^{18}O_{corrected\text{-}diatom} = (\delta^{18}O_{diatom} - \delta^{18}O_{contamination} \times [\%_{contamination} / 100]) / (\%_{diatom} / 100) \quad (1)$$

where $\delta^{18}O_{diatom}$ is the original isotope value of the prepared diatom sample, $\%_{contamination}$ and $\%_{diatom}$ are calculated using Eq. 2 (details below) and $\delta^{18}O_{contamination}$ is the isotope value of contamination.

A number of modifications were made to the methodology for the contamination correction of $\delta^{18}O_{diatom}$ samples that was previously used for Nar Gölü sediments (Dean

et al., 2013) to make it more robust. For element concentration data, here we use an XRF (Panalytical εpsilon 3 XL) rather than an Energy-Dispersive X-ray Spectroscopy (EDS) probe, allowing for more precise measurements of aluminium concentrations (a good marker for the amount of detrital silicates present (Mackay et al., 2011)), with an analytical reproducibility of 0.03%. The XRF was set up to quantify the proportions of Na, Mg, Al, Si, P, S, K, Ca, T, Mn and Fe using the Panalytical Omnian program. Instead of calculating the $\delta^{18}O$ of contamination through the intercept of the $\delta^{18}O_{diatom}$ vs. contamination plot, nine turbidites from along the NAR10 core were prepared and run in the same way as the diatom isotope samples. They had a mean $\delta^{18}O$ value of 16.0‰ (±1.0‰), which is within uncertainty of the value of 16.5‰ estimated in Dean et al. (2013) from NAR01/02. It is likely that % contamination was overestimated in Dean et al. (2013) because some minerogenic contamination will be removed by the first fluorination stage before $\delta^{18}O$ is measured (Swann and Leng, 2009) and diatom frustules can incorporate aluminium, so Al_2O_3% in the samples does not only reflect minerogenic contamination (Beck et al., 2002; Koning et al., 2007; Swann, 2010; Ren et al., 2013). To investigate the latter effect, Scanning Electron Microscopy (SEM) was used to identify individual clean diatoms (i.e. with no detrital silicates visible at all) and the Al_2O_3 wt% of the individual diatoms was measured by EDS, averaging 1.0% ±0.4 (1σ) for the individual diatoms measured across 16 samples. This suggests that there is a significant amount of diatom-bound aluminium, so a correction factor was applied to

account for this. Based on the average Al_2O_3 value of the turbidite layers throughout the core sequence that were prepared and run as $\delta^{18}O_{diatom}$ samples, 14.56% Al_2O_3 represents 100% contamination (i.e. all detrital silicates, no diatoms). 1‰ Al_2O_3 represents 0% contamination. Thus, there is an equation, derived from Figure SI-1, that can be used to calculate the new $\%_{contamination}$ values for our samples:

$$\%_{contamination} = (7.3746 \times sample_{Al}) - 7.3746 \quad (2)$$

where $sample_{Al}$ is the measured Al_2O_3 concentration in each sample analysed for $\delta^{18}O_{diatom}$. Eq. 2 was used to calculate the $\%_{contamination}$ values for Eq. 1. This modified methodology was used on the new samples from NAR10, as well as to recalculate the corrections to the NAR01/02 data presented in Dean et al. (2013). Henceforth, $\delta^{18}O_{diatom}$ refers to the corrected $\delta^{18}O_{diatom}$ data.

Uncertainties from individual components of the correction are outlined in Table 1 and were combined to calculate the overall uncertainty associated with the correction. Uncertainties are reduced compared to those reported in Dean et al. (2013) because of the improved methodology. Figure SI-2 shows the original corrected NAR01/02 data published in Dean et al. (2013) compared to re-calculated values used in this paper. Although the actual values are slightly different and not all of the samples from Dean et

al. (2013) had sufficient material remaining for re-analysis by XRF (so data are now excluded), the general trends are very similar, with periods of lower $\delta^{18}O$ particularly at 1,450, 1,250 and 120 years BP. The overall similarities in trends mean that the interpretations of Dean et al. (2013) are still valid, although for consistency in this paper we present the re-analysed NAR01/02 data along with the NAR10 data.

3.3 Calculating $\delta^{18}O_{lakewater}$

To allow for direct comparison of the $\delta^{18}O$ data from carbonates and diatoms, we estimate $\delta^{18}O_{lakewater}$ at the time of carbonate precipitation and diatom growth using the calcite (Kim and O'Neil, 1997), aragonite (Grossman and Ku, 1986) and diatom (Crespin et al., 2010) palaeotemperature equations respectively:

$$\delta^{18}O_{lakewater} = \delta^{18}O_{calcite} - (4.58 \pm [4.58^2 - 4 \times 0.08 \times (13.8 - T)]^{1/2})/ 2 \times 0.08 \quad (3)$$

$$\delta^{18}O_{lakewater} = \delta^{18}O_{aragonite} - (T - 19.7)/-4.34 \quad (4)$$

$$\delta^{18}O_{lakewater} = \delta^{18}O_{diatom} - (T - 245)/-6.25 \quad (5)$$

where $\delta^{18}O_{lakewater}$ and $\delta^{18}O_{diatom}$ are expressed on the VSMOW scale, $\delta^{18}O_{calcite}$ and $\delta^{18}O_{aragonite}$ against VPDB and T in °C. We use a temperature range of +15 to +20°C for the time of carbonate precipitation and +5 to +10°C for the time of diatom growth, justified by our measurements of seasonal lake waters from 2011-2013 (Figure 2 and Eastwood et al., unpublished data). The temperature range for the time of diatom growth has been reduced from that used in Dean et al. (2013), where we estimated +5 to +15°C, because of our increased knowledge of intra-annual epilimnion temperature variability with the additional years of temperature logging data from Nar Gölü. While we recognise that there will have been changes in temperature during the Holocene, these changes are likely to have been only a few degrees centigrade (see references in section 5.1), smaller than the ranges of 5°C given for the times of diatom growth and carbonate precipitation.

3.4 Lake isotope mass balance models

To examine further the changes in hydroclimate seasonality and how this would be recorded in the seasonality of the lake $\delta^{18}O$ system, we use an isotope mass balance model, employing the equations outlined in Jones and Imbers (2010) and Jones et al. (2016), and fully explained in the Supplementary Information. The equations are based on monthly time steps to allow investigations of changing intra-annual $\delta^{18}O_{lakewater}$

239 variability under different climatic states that have been identified from the isotope data:
240 for the present day (Modern), the Mid Holocene (here meaning from approximately
241 6,000 to 1,600 years BP) and the Early Holocene.
242
243 For the present day, average monthly values of temperature (average [Tav], minimum
244 [Tmin] and maximum [Tmax]), total precipitation (P) and snowfall between 2005 and
245 2011 (only until 2010 for snowfall) from the meteorological station at Niğde were used
246 to drive a model of modern conditions in a lake with the same volume (~750,000 m^3)
247 and lake area (556,500 m^2) as Nar Gölü (Table 2 and Supplementary Information).
248
249 In this modern lake setting, annual average $\delta^{18}O_{lakewater}$ in the model is 0.59‰ with a
250 range (intra-annual $\delta^{18}O_{lakewater}$ variability) of 1.06 (Table 2). This compares to
251 measured summer values at Nar Gölü of between –1.9 and –0.2‰ for the same period
252 (2005-2011), and an intra-annual range of ~1.6‰ (Dean et al., 2015a). The difference
253 between the measured data and the model are due to a number of factors. Firstly, the
254 model is for a lake in Niğde, the location of the nearest meteorological station, not for
255 Nar Gölü. This will affect the precipitation and evaporation components of the model,
256 and therefore the parameterisation of surface and groundwater inflow and outflow,
257 which have narrow windows for a given lake in a given location (Jones et al., 2016).
258 Nar Gölü is also stratified, adding a level of complexity to the isotope hydrology not

included in the model. However, the model in the Modern scenario has mean and intra-annual $\delta^{18}O$ values in the same order as Nar Gölü, and is used here not to recreate conditions at Nar Gölü precisely, but to inform our discussion of why $\delta^{18}O$ may change in time. As such, the model is deliberately simple, and appropriate. Inputs to the model for the palaeoclimate scenarios are based on our best understanding of regional temperature and precipitation changes from the literature (see discussions below).

4 Results

Figure 3 shows $\delta^{18}O_{carbonate}$ and $\delta^{18}O_{diatom}$ plotted against depth. There are gaps in both the $\delta^{18}O_{carbonate}$ record, where interpretation of $\delta^{18}O_{carbonate}$ values is complicated by dolomite precipitation (Dean et al., 2015b), and the $\delta^{18}O_{diatom}$ record, because there was not enough diatom silica for isotope analysis and/or samples were too contaminated (with detrital silicates and at times additionally with dolomite), even after cleaning, to run. Because of issues with the chronology discussed elsewhere (Dean et al., 2015b; Roberts et al., 2016), the data between 1034-1161 cm are not plotted on Figure 4.

Figure 3

Figure 4

279

280 The overall trends in $\delta^{18}O_{carbonate}$ and $\delta^{18}O_{diatom}$ are similar. Both have lower values
281 towards the bottom of the core in the period likely to be at the time of the Bølling-
282 Allerød, higher values at the time of the Younger Dryas, and lower values in the early
283 Holocene (Figure 4). Both $\delta^{18}O_{diatom}$ and $\delta^{18}O_{carbonate}$ increase at ~7,500 years BP to
284 higher values (by 4‰ VSMOW for $\delta^{18}O_{diatom}$ and ~5‰ VPDB for $\delta^{18}O_{carbonate}$).
285 However, a major difference is that while there is another increase in $\delta^{18}O_{carbonate}$ (>2‰
286 VPDB) ~4,100 years BP, ending with peak Holocene values that are maintained until
287 ~1,600 years BP, there is no corresponding second increase in $\delta^{18}O_{diatom}$ values. Where
288 data are available, $\delta^{18}O_{diatom}$ values are relatively stable, at c.+37‰ VSMOW for the
289 period ~7,000 to 1,600 years BP after rising from early Holocene values of c.+33‰.
290 Both $\delta^{18}O_{carbonate}$ and $\delta^{18}O_{diatom}$ decline dramatically at ~1,600 years BP for ~400 years,
291 before returning to higher values for most of the last 1,000 years.

292

293 Figure 4 also shows $\delta^{18}O_{lakewater}$ estimated for the times of diatom growth and carbonate
294 precipitation. Because late glacial temperatures are not well known, we only use the
295 palaeotemperature equations to reconstruct $\delta^{18}O_{lakewater}$ for the Holocene, during which
296 annual average temperatures probably only changed by a few degrees in the region (e.g.
297 Emeis et al., 2000). The shaded areas on Figure 4C combine maximum and minimum
298 $\delta^{18}O_{lakewater}$ values possible for the temperature ranges noted above, plus the

uncertainties associated with the $\delta^{18}O_{diatom}$ contamination correction. $\delta^{18}O_{lakewater}$ at the time of diatom growth increased from c.–5‰ in the early Holocene to c.–1‰ in the mid Holocene, before falling to c.–15‰ ~1,600-1,200 years BP and then returning to higher values (c.–2 to –3‰) for the last 1,000 years. $\delta^{18}O_{lakewater}$ at the time of carbonate precipitation increased from c.–3‰ in the early Holocene to c.+1‰ ~6,600 years BP and to c.+3‰ by ~4,000 years BP, before falling to c.–4‰ ~1,600-1,200 years BP and then increasing to c.–1‰ for the last 1,000 years.

$\Delta\delta^{18}O_{lakewater}$, the difference between $\delta^{18}O_{lakewater}$ at the time of carbonate precipitation compared to the time of diatom growth, was only ~1‰ in the early Holocene. It then increased to ~4‰ for much of the time from ~4,100 to 1,600 years BP, as $\delta^{18}O_{lakewater}$ at the time of carbonate precipitation increased 4,100 years BP, but $\delta^{18}O_{lakewater}$ at the time of diatom growth did not (Figure 4C). Then, ~1,600-1,200 years BP, because the fall in $\delta^{18}O_{diatom}$ is much greater than the fall in $\delta^{18}O_{carbonate}$, $\Delta\delta^{18}O_{lakewater}$ values are >10‰. For the last 1,000 years, $\Delta\delta^{18}O_{lakewater}$ declined to levels more similar to the early Holocene. Limited variability in recent times is also shown in our monitoring data, with only a 0.5‰ difference in our lakewater samples between April and July in 2012 (Figure 2) and a 0.7‰ difference seen between April and August 2002 (Jones et al., 2005).

5 Discussion

From the isotope data, there appear to be three key lake states: 1. limited difference between $\delta^{18}O_{lakewater}$ at the times of diatom growth and carbonate precipitation, i.e. $\Delta\delta^{18}O_{lakewater}$ ~1‰ (during the early Holocene and last 1,000 years); 2. intermediate $\Delta\delta^{18}O_{lakewater}$, at ~4‰ (mid Holocene and up to ~1,600 years BP), and 3. maximum $\Delta\delta^{18}O_{lakewater}$, at ~10‰ (~1,600-1,200 years BP). We discuss these in turn. The differences in resolution between the carbonate and diatom isotope data means that we limit ourselves to comparing the long-term general trends in the data through the early and mid Holocene.

5.1 The early Holocene (11,700 to 6,500 years BP)

$\delta^{18}O_{diatom}$ and $\delta^{18}O_{carbonate}$ values for the early Holocene are both low relative to the mid and late Holocene (Figure 4), which could indicate higher annual average P/E (i.e. effectively wetter conditions) in the early Holocene, as has been suggested by other studies (summarised in Roberts et al., 2008). Specifically, pollen data (Djamali et al., 2010; Kotthoff et al., 2008; Peyron et al., 2011; Peyron et al., 2017), microcharcoal data (Wick et al., 2003; Turner et al., 2008; Vanniere et al., 2011), climate modelling results (Brayshaw et al., 2010) and $\delta^{18}O$ data of freshwater mollusc shells from Çatalhöyük

339 ~160 km SW of Nar (Bar-Yosef Mayer et al., 2012; Lewis et al., 2017) have suggested
340 that the early Holocene in the Eastern Mediterranean region had wetter winters than
341 present, but with many of the studies suggesting drier springs and/or summers. Annual
342 average temperatures were several degrees cooler in the early Holocene compared to the
343 late Holocene, as reconstructed by alkenone-derived sea surface temperatures (Emeis et
344 al., 2000; Triantaphyllou et al., 2009) and speleothem fluid inclusions (McGarry et al.,
345 2004). However, the prominence of *Pistacia* in the pollen record from Nar Gölü
346 (Roberts et al., 2016) and from nearby Eski Acıgöl (Roberts et al., 2001; Woldring and
347 Bottema, 2003), between 11,000 and 8,000 years BP, suggests winters were milder than
348 today (Rossignol-Strick, 1999). Therefore, the inferred drops in annual temperature may
349 have been concentrated in the summer. There is, however, a gap in the $\delta^{18}O_{diatom}$ record
350 between 8,800 and 7,900 years BP due to there being too little diatom silica for diatom
351 isotope measurements to be made. Intriguingly, this period coincides with a phase of
352 marked spring floods on the Çarşamba river in Anatolia (Boyer et al., 2006), which
353 would have been caused by enhanced spring snowmelt in its upper watershed in the
354 Taurus mountains. Despite the fact that spring and summer precipitation may have been
355 lower in the early Holocene than the present day, $\delta^{18}O_{carbonate}$ is still lower in the early
356 Holocene and there is limited $\Delta\delta^{18}O_{lakewater}$. Presumably, the lower $\delta^{18}O_{carbonate}$ and
357 limited $\Delta\delta^{18}O_{lakewater}$ is due to relatively less summer evaporation of the lake waters
358 compared to the mid and late Holocene, which is to be expected if there were lower

359 temperatures in the early Holocene spring/summer, as well as increased winter
360 precipitation. Our mass balance modelling allows us to refine our basic interpretation of
361 hydroclimate in the early Holocene.
362
363 In our early Holocene model, we have reduced the annual average temperature by 1°C,
364 as estimated from the studies cited above and as used in Jones et al. (2007); details in SI
365 Tables. Annual precipitation values are kept the same as the present day, but the
366 seasonal distribution has been shifted to more winter-dominated with no snow, as is
367 indicated by the literature discussed above. Under this scenario, average annual lake
368 water values are lower than the present day model (–2.81‰), and could be even more so
369 if annual-averaged precipitation was increased under the same P/E seasonality regime,
370 as seems possible (Roberts et al., 2008). This demonstrates that the seasonality of P/E,
371 in addition to the average annual conditions, is important in controlling inter-annual
372 changes in $\delta^{18}O_{lakewater}$.
373
374 To investigate further the relative contributions of precipitation and temperature (linked
375 closely to evaporation in this model), an early Holocene scenario, using modern day
376 temperatures (as well as modern day annual-average precipitation levels again) and
377 changing only the seasonal distribution of precipitation, was also undertaken. Here
378 $\delta^{18}O_{lakewater}$ was still lower than the present day scenario (–0.57‰) and the average of

379 monthly P/E increases (Table 2). This result drives a difference in this model because
380 groundwater inflow and outflow are dependent on P/E, with additional groundwater
381 outflow required in the early Holocene compared to present day to balance the lake
382 system, and suggesting higher lake levels under early Holocene conditions. This
383 indicates that changing the seasonal distribution of P/E, irrespective of annual average
384 conditions, can lead to changes in both lake hydrology and lake isotope composition. It
385 highlights the need to be careful when suggesting that the early Holocene was 'wetter'
386 than the mid and late Holocene based solely on evidence from lake sediment isotopes,
387 as now it is clear that changes in the seasonality of P/E have an impact on $\delta^{18}O$, in part
388 due to changes in seasonal water balance as well as due to changes in $\delta^{18}O$ of
389 precipitation (Table 2), as suggested by Stevens et al. (2001, 2006) for Lakes Zeribar
390 and Mirabad.
391
392 *5.2 The mid Holocene (~6,500 to ~1,600 years BP)*
393
394 At Nar Gölü, a number of proxies respond to changes in lake level, usually driven by
395 changes in P/E, such as lithology (varved vs. non-varved), carbonate mineralogy (calcite
396 vs. aragonite and dolomite) (Dean et al., 2015b), the Sr-Ca elemental ratio and certain
397 diatom species (Roberts et al., 2016). These multiple proxies indicate that annual
398 average P/E was probably lower after ~6,500 years BP compared to the early Holocene.

399 We know at Nar Gölü that lake level falls lead to more positive $\delta^{18}O_{carbonate}$ (Dean et al.,
400 2015a) and therefore a significant part of the $\delta^{18}O$ trend in carbonates and diatoms to
401 higher values in the mid and late Holocene, compared to the early Holocene, is likely
402 related to a shift to drier conditions. Other influences on $\delta^{18}O$, such as changes in the
403 isotopic composition of the source of precipitation, amount effect or temperature, could
404 not have accounted for the large size of the shift in both $\delta^{18}O_{carbonate}$ and $\delta^{18}O_{diatom}$ from
405 the early to mid and late Holocene.
406
407 $\Delta\delta^{18}O_{lakewater}$ does not initially increase in the mid Holocene because both $\delta^{18}O_{carbonate}$
408 and $\delta^{18}O_{diatom}$ increase, but in the period ~4,100 to ~1,600 years BP $\delta^{18}O_{lakewater}$ at the
409 time of diatom growth is up to ~4‰ lower than at the time of carbonate precipitation
410 (Figure 4). Annual average precipitation must have been lower for most of the mid and
411 late Holocene compared to the early Holocene (Jones et al., 2007). It is possible that a
412 significant share of this precipitation decline occurred ~7,500 years BP, while at ~4,100
413 years BP there was a rise in summer evaporation but winter/spring precipitation levels
414 did not change substantially. If that was the case, that would explain why both $\delta^{18}O_{diatom}$
415 (responding more to winter/spring precipitation) and $\delta^{18}O_{carbonate}$ (responding more to
416 summer evaporation) increased ~7,500 years BP but only $\delta^{18}O_{carbonate}$ increased at
417 ~4,100 years BP (thus leading to increased $\Delta\delta^{18}O_{lakewater}$). However, lake level change
418 could account for some of this increased $\Delta\delta^{18}O_{lakewater}$. $\Delta\delta^{18}O_{lakewater}$ will be more

419 sensitive to inputs and outputs when the lake level and volume were lower, with less of
420 a buffering effect than when the lake level is higher: this is a well-known phenomenon
421 in limnology (e.g. Leng and Anderson, 2003; Steinman et al., 2010).
422
423 To test this with the lake isotope mass balance model, two model conditions are set for
424 this period. In both, precipitation is reduced compared to the present day as multi-proxy
425 evidence from Nar Gölü (Dean et al., 2015b; Roberts et al., 2016) and elsewhere in the
426 region (Roberts et al., 2008) points to lower lake levels at this time. In the first Mid
427 Holocene scenario (MHi), temperatures are held the same as the present day, resulting
428 in an average $\delta^{18}O_{lakewater}$ value of +1.06‰, which is higher than the early Holocene
429 scenarios and thus supports our contention that some of the increase in $\delta^{18}O$ could be
430 due to reduced annual precipitation. However, the range in the model is only 1.10‰
431 (Table 2), which is similar to the early Holocene model, despite the higher $\Delta\delta^{18}O_{lakewater}$
432 seen in the data in the mid Holocene compared to the early Holocene. In the second Mid
433 Holocene scenario (MHii), summer temperatures are raised to increase summer
434 evaporation such that P/E seasonality is increased relative to MHi. Average $\delta^{18}O_{lakewater}$
435 values become even more positive (+2.00‰) and the range increases (1.22‰; Table 2).
436 Further, a shift from a steady state lake with the same volume as the present day
437 scenario, in MHii conditions, to one with a 20% smaller volume, increases the intra-

annual $\delta^{18}O_{lakewater}$ range to 1.52‰, showing how a change to lower lake levels could account for some of the increase in $\Delta\delta^{18}O_{lakewater}$ at this time (as discussed above).

To ensure steady state lakes under the mid Holocene climatic scenarios, the groundwater outflow constant has to be reduced (see Supplementary Information for model details). In the model, this is partly a function of P/E as more water entering the lake will push more of it out, however here it needs to be further reduced relative to present day to ensure a steady state lake, i.e. one where volume is not always increasing or decreasing at an annual time step. This suggests there are further controls on groundwater outflow that are not described by our simple model, possibly linked to lake volume and depth, with the lower lake levels of the mid Holocene also potentially contributing to reduced groundwater outflow at these times.

5.2.3 Late Holocene (last 1,600 years)

Around 1,600-1,200 years BP, $\Delta\delta^{18}O_{lakewater}$ was at times >10‰. Dean et al. (2013) hypothesised that this was due to a seasonal freshwater lid of low $\delta^{18}O$ snowmelt occurring at this time, in which the diatoms lived. To further investigate the sensitivity of the Nar Gölü system to snow volume, the modern lake isotope mass balance model was altered to have no snow, or double the amount of snow, keeping all other variables

458 the same. This produced more positive or more negative annual average $\delta^{18}O_{lakewater}$
459 values respectively, as would be expected by putting less or more negative $\delta^{18}O$ water
460 into the system (Table 2). There is no impact on the range if these changes are made
461 into a well-mixed lake system as in the model, further suggesting that density
462 differences and stratification are probably important in explaining the $\Delta\delta^{18}O_{lakewater}$
463 variability reconstructed down-core at Nar Gölü as proposed by Dean et al. (2013) for
464 this unusual period during the late Holocene.
465

466 **6 Conclusions**

467

468 The combination of two $\delta^{18}O$ records, from diatoms and endogenic carbonate that
469 formed in Nar Gölü in central Turkey at different times of the year, helps to inform
470 discussion of palaeoseasonality. Our record indicates that there are three lake states
471 through the Holocene: the early Holocene and the last 1,000 years when there is limited
472 $\Delta\delta^{18}O_{lakewater}$, the mid Holocene and up to ~1,600 years BP when $\Delta\delta^{18}O_{lakewater}$ was at
473 times ~4‰ and a short period ~1,600-1,200 years BP when $\Delta\delta^{18}O_{lakewater}$ was ~10‰.
474 Modelling results indicate that the increase in $\Delta\delta^{18}O_{lakewater}$ from the early to the mid
475 Holocene could be related to changes in P/E seasonality, but a shift to lower lake levels
476 (and volumes) would have amplified the impact of any changes in P/E. Therefore,
477 while we have shown that using $\Delta\delta^{18}O_{lakewater}$ to compare lake conditions at different

478 times of the year can provide insights into seasonality, it is not a simple proxy for intra-
479 annual P/E variability. In terms of inter-annual $\delta^{18}O$ change, we suggest that lower
480 $\delta^{18}O_{carbonate}$ and $\delta^{18}O_{diatom}$ values in the early Holocene compared to the present day
481 could partly be the result of changes in the seasonality of P/E. However, the multi-proxy
482 evidence available from Nar Gölü clearly points to a mid Holocene transition to lower
483 lake levels driven by annual-mean shifts to reduced P/E.
484
485 **Acknowledgments**
486
487 JRD was funded by NERC PhD studentship NE/I528477/1 (2010-2014). Diatom
488 isotope work was funded by NIGFSC grant IP/1346/1112 to MDJ. Fieldwork was
489 supported by National Geographic and British Institute at Ankara grants to CNR. All
490 authors have contributed intellectually and approved the final version. We would like to
491 thank those others who contributed to field work in 2010 at Nar Gölü: Samantha
492 Allcock, Hakan Yiğitbaşıoğlu, Fabien Arnaud, Emmanuel Malet, Ersin Ateş, Çetin
493 Şenkul, Gwyn Jones, Ryan Smith and Ceran Şekeryapan. George Swann is thanked for
494 his useful advice with the diatom isotope corrections. We thank Gianni Zanchetta and
495 an anonymous reviewer for helpful comments that improved the manuscript. A
496 Supplementary Information file and a data file are associated with the online version of
497 this paper.

498

499 **References**

500

501 Bar-Yosef Mayer DE, Leng MJ, Aldridge DC, Arrowsmith C, Gumus BA and Sloane
502 HJ (2012) Modern and early-middle Holocene shells of the freshwater mollusc
503 Unio, from Catalhoyuk in the Konya Basin, Turkey: preliminary palaeoclimatic
504 implications from molluscan isotope data. *Journal of Archaeological Science* 39:
505 76-83.
506 Beck L, Gehlen M, Flank AM, Van Bennekom AJ and Van Beusekom JEE (2002) The
507 relationship between Al and Si in biogenic silica as determined by PIXE and
508 XAS. *Nuclear Instruments & Methods in Physics Research Section B - Beam*
509 *Interactions with Materials and Atoms* 189: 180-184.
510 Boyer P, Roberts N and Baird D (2006) Holocene environment and settlement on the
511 Çarşamba alluvial fan, South Central Turkey: Integrating Geoarchaeology and
512 Archaeological Field Survey. *GeoArchaeology* 21: 675-699.
513 Brayshaw D, Hoskins B and Black E (2010) Some physical drivers of change in the
514 winter storm tracks over the Atlantic and Mediterranean during the Holocene.
515 *Philosophical Transactions of the Royal Society of London* 368: 5185-5223.
516 Chapligin B, Leng MJ, Webb E, Alexandre A, Dodd JP, Ijiri A, Lücke A, Shemesh A,
517 Abelmann A, Herzschuh U, Longstaffec FJ, Meyer H, Moschen R, Okazaki Y,

518 Rees NH, Sharp ZD, Sloane HJ, Sonzogni C, Swann GEA, Sylvestre F, Tyler JJ
519 and Yam R (2011) Inter-laboratory comparison of oxygen isotope compositions
520 from biogenic silica. *Geochimica et Cosmochimica Acta* 75: 7242-7256.
521 Crespin J, Sylvestre F, Alexandre A, Sonzogni C, Pailles C and Perga ME (2010) Re-
522 examination of the temperature-dependent relationship between delta O-
523 18(diatoms) and delta O-18(lake water) and implications for paleoclimate
524 inferences. *Journal of Paleolimnolgy* 44: 547-557.
525 Darling WG, Bath AH, Gibson JJ and Rozanski K (2006) Isotopes in Water. In: Leng
526 MJ (ed) *Isotopes in Palaeoenvironmental Research*. Dordrecht: Springer.
527 Dean JR, Eastwood WJ, Roberts CN, Jones MD, Yigitbasioglu H, Allcock SL,
528 Woodbridge J, Metcalfe SE and Leng MJ (2015a) Tracking the hydro-climatic
529 signal from lake to sediment: a field study from central Turkey. *Journal of*
530 *Hydrology* 529: 608-621.
531 Dean JR, Jones MD, Leng MJ, Noble SR, Metcalfe SE, Sloane HJ, Sahy D, Eastwood
532 WJ and Roberts CN (2015b). Eastern Mediterranean hydroclimate over the late
533 glacial and Holocene, reconstructed from the sediments of Nar lake, central
534 Turkey, using stable isotopes and carbonate mineralogy. *Quaternary Science*
535 *Reviews* 124: 162-174.
536 Dean JR, Jones MD, Leng MJ, Sloane HJ, Roberts CN, Woodbridge J, Swann GEA,
537 Metcalfe SE, Eastwood WJ and Yigitbasioglu H (2013) Palaeo-seasonality of the

last two millennia reconstructed from the oxygen isotope composition of carbonates and diatom silica from Nar Gölü, central Turkey. *Quaternary Science Reviews* 66: 35-44.

Djamali M, Akhani H, Andrieu-Ponel V, Braconnot P, Brewer S, de Beaulieu JL, Fleitmann D, Fleury J, Gasse F, Guibal F, Jackson ST, Lezine AM, Medail F, Ponel P, Roberts N and Stevens L (2010) Indian Summer Monsoon variations could have affected the early-Holocene woodland expansion in the Near East. *The Holocene* 20: 813-820.

Emeis KC, Struck U, Schulz HM, Rosenberg R, Bernasconi S, Erlenkeuser H, Sakamoto T and Martinez-Ruiz F (2000) Temperature and salinity variations of Mediterranean Sea surface waters over the last 16,000 years from records of planktonic stable oxygen isotopes and alkenone unsaturation ratios. *Palaeogeography Palaeoclimatology Palaeoecology* 158: 259-280.

England A, Eastwood WJ, Roberts CN, Turner R, Haldon JF (2008) Historical landscape change in Cappadocia (central Turkey): a palaeoecological investigation of annually laminated sediments from Nar lake. *The Holocene* 18: 1229-1245.

Gevrek A and Kazanci N (2000) A Pleistocene, pyroclastic-poor maar from central Anatolia, Turkey: influence of a local fault on a phreatomagmatic eruption. *Journal of Volcanology and Geothermal Research* 95: 309-317

558 Grossman EL and Ku TL (1986) Oxygen and carbon isotope fractionation in biogenic
559 aragonite - temperature effects. *Chemical Geology* 59: 59-74.
560 Issar A and Adar E (2010) Progressive development of water resources in the Middle
561 East for sustainable water supply in a period of climate change. *Philosophical*
562 *Transactions of the Royal Society A - Mathematical Physical and Engineering*
563 *Sciences* 368: 5339-5350.
564 Jones MD, Cuthbert MO, Leng MJ, McGowan S, Mariethoz G, Arrowsmith C, Sloane
565 HJ, Humphrey KK and Cross I (2016) Comparisions of observed and modelled
566 lake $\delta^{18}O$ variability. *Quaternary Science Reviews* 131: 329-340.
567 Jones MD and Imbers J (2010) Modelling Mediterranean lake isotope variability.
568 *Global and Planetary Change* 71: 193-200.
569 Jones MD, Leng MJ, Roberts CN, Turkes M and Moyeed R (2005) A coupled
570 calibration and modelling approach to the understanding of dry-land lake oxygen
571 isotope records. *Journal of Paleolimnology* 34: 391-411.
572 Jones MD and Roberts CN (2008) Interpreting lake isotope records of Holocene
573 environmental change in the Eastern Mediterranean. *Quaternary International* 181: 32-
574 38.
575 Jones MD, Roberts CN and Leng MJ (2007) Quantifying climatic change through the
576 last glacial-interglacial transition based on lake isotope palaeohydrology from
577 central Turkey. *Quaternary Research* 67: 463-473.

578 Jones MD, Roberts CN, Leng MJ and Türkeş M (2006) A high-resolution late Holocene
579 lake isotope record from Turkey and links to North Atlantic and monsoon climate.
580 *Geology* 34: 361-364.
581 Kelley CP, Mohtadi S, Cane MA, Seager R and Kushnir Y (2015) Climate change in
582 the Fertile Crescent and implications of the recent Syrian drought. *Proceedings of*
583 *the National Academy of Sciences* 112: 3241-3246.
584 Kim ST and O'Neil JR (1997) Equilibrium and nonequilibrium oxygen isotope effects
585 in synthetic carbonates. *Geochimica et Cosmochimica Acta* 61: 3461-3475.
586 Koning E, Gehlen M, Flank AM, Calas G and Epping E (2007) Rapid post-mortem
587 incorporation of aluminum in diatom frustules: evidence from chemical and
588 structural analyses. *Marine Chemistry* 106: 208-222.
589 Kotthoff U, Prodd J, Müller UC, Peyron O, Schmiedl G, Schulz H and Bordon A (2008)
590 Climate dynamics in the borderlands of the Aegean Sea during formation of
591 sapropel S1 deduced from a marine pollen record. *Quaternary Science Reviews*
592 27: 832-845.
593 Kutiel H and Türkeş M (2005) New evidence for the role of the North Sea-Caspian
594 Pattern on the temperature and precipitation regimes in continental Central
595 Turkey. *Geografiska Annaler Series A - Physical Geography* 87A: 501-513.
596 Leng MJ and Anderson AJ (2003) Isotopic variation in modern lake waters from
597 western Greenland. *The Holocene* 13: 605-611.Leng MJ and Sloane HJ (2008).

598 Combined oxygen and silicon isotope analysis of biogenic silica. *Journal of*
599 *Quaternary Science* 23: 313-319.
600 Lewis JP, Leng MJ, Dean JR, Marciniak A, Bar-Yosef Mayer DE and Wu X (2017)
601 Early Holocene palaeoseasonality inferred from the stable isotope composition of
602 Unio shells from Çatalhöyük, Turkey. *Environmental Archaeology* 1: 79-95.
603 Mackay AW, Swann GEA, Brewer TS, Leng MJ, Morley DW, Piotrowska N, Rioual P.
604 and White D (2011) A reassessment of late glacial-Holocene diatom oxygen
605 isotope record from Lake Baikal using a geochemical mass-balance approach.
606 *Journal of Quaternary Science* 26: 627-634.
607 McGarry S, Bar-Matthews M, Matthews A, Vaks A, Schilman B and Ayalon A (2004)
608 Constraints on hydrological and paleotemperature variations in the Eastern
609 Mediterranean region in the last 140 ka given by the delta D values of speleothem
610 fluid inclusions. *Quaternary Science Reviews* 23: 919-934.
611 Morley DW, Leng MJ, Mackay AW, Sloane HJ, Rioual P and Battarbee RW (2004)
612 Cleaning of lake sediment samples for diatom oxygen isotope analysis. *Journal of*
613 *Paleolimnology* 31: 391-401.
614 Peyron O, Combourieu-Nebout N, Brayshaw D, Goring S, Andrieu-Ponel V, Desprat S,
615 Fletcher W, Gambin B, Ioakim C, Joannin S, Kotthoff U, Kouli K, Montade V,
616 Pross J, Sadori L and Magny M (2017). Precipitation changes in the

617 Mediterranean basin during the Holocene from terrestrial and marine pollen
618 records: a model-data comparision. Climate of the Past 13: 249-265.
619 Peyron O, Goring S, Dormoy I, Kotthoff U, Pross J, De Beaulieu JL, Drescher-
620 Schneider R, Vanniere B and Magny M (2011) Holocene seasonality changes in
621 the central Mediterranean region reconstructed from the pollen sequences of Lake
622 Accesa (Italy) and Tenaghi Philippon (Greece). *The Holocene* 21: 131-146.
623 Ren H, Brunelle BG, Sigman DM and Robinson RS (2013) Diagenetic aluminum
624 uptake into diatom frustules and the preservation of diatom-bound organic
625 nitrogen. *Marine Chemistry* 155: 92-101.
626 Roberts CN, Allcock SL, Arnaud F, Dean JR, Eastwood WJ, Jones MD, Leng MJ,
627 Metcalfe SE, Malet E, Woodbridge J and Yiğitbaşıoğlu H (2016) A tale of two
628 lakes: a multi-proxy comparison of Late Glacial and Holocene environmental
629 change in Cappadocia, Turkey. *Journal of Quaternary Science* 31: 348-362.
630 Roberts N, Jones MD, Benkaddour A, Eastwood WJ, Filippi ML, Frogley MR, Lamb
631 HF, Leng MJ, Reed JM, Stein M, Stevens L, Valero-Garces B and Zanchetta G
632 (2008) Stable isotope records of Late Quaternary climate and hydrology from
633 Mediterranean lakes: the ISOMED synthesis. *Quaternary Science Reviews* 27:
634 2426-2441.
635 Roberts N, Reed JM, Leng MJ, Kuzucuoğlu C, Fontugne M, Bertaux J, Woldring H,
636 Bottema S, Black S, Hunt, E and Karabiyikoglu M (2001) The tempo of Holocene

climatic change in the eastern Mediterranean region: new high-resolution crater-lake sediment data from central Turkey. *The Holocene* 11: 721-736.

Rohling EJ (2016) Of lakes and fields: A framework for reconciling palaeoclimatic drought inferences with archaeological impacts. *Journal of Archaeological Science* 73: 17-24.

Rossignol-Strick M (1999) The Holocene climatic optimum and pollen records of sapropel 1 in the eastern Mediterranean, 9000-6000 BP. *Quaternary Science Reviews* 18: 515-530.

Steinman BA, Rosenmeier MF and Abbott MB (2010) The isotopic and hydrologic response of small, close-basin lakes to climate forcing from predictive models: simulations of stochastic and mean state precipitation variations. *Limnology and Oceanography* 55: 2246-2261.

Stevens LR, Ito E, Schwalb A and Wright HE (2006) Timing of atmospheric precipitation in the Zagros Mountains inferred from a multi-proxy record from Lake Mirabad, Iran. *Quaternary Research* 66: 494-500.

Stevens LR, Wright HE and Ito E (2001) Proposed changes in seasonality of climate during the Lateglacial and Holocene at Lake Zeribar, Iran. *The Holocene* 11: 747-755.

655 Swann GEA (2010) A comparison of the Si/Al and Si/time wet-alkaline digestion
656 methods for measurement of biogenic silica in lake sediments. *Journal of*
657 *Paleolimnology* 44: 375-385.
658 Swann GEA and Leng MJ (2009) A review of diatom delta O-18 in palaeoceanography.
659 *Quaternary Science Reviews* 28: 384-398.
660 Triantaphyllou MV, Ziveri P, Gogou A, Marino G, Lykousis V, Bouloubassi I, Emeis
661 KC, Kouli K, Dimiza M, Rosell-Mele A, Papanikolaou M, Katsouras G and
662 Nunez N (2009) Late Glacial-Holocene climate variability at the south-eastern
663 margin of the Aegean Sea. *Marine Geology* 266: 182-197.
664 Turner R, Roberts N, Eastwood WJ, Jenkins E and Rosen A (2010) Fire, climate and the
665 origins of agriculture: micro-charcoal records of biomass burning during the last
666 glacial-interglacial transition in Southwest Asia. *Journal of Quaternary Science*
667 25: 371-386.
668 Turner R, Roberts N and Jones MD (2008) Climatic pacing of Mediterranean fire
669 histories from lake sedimentary microcharcoal. *Global and Planetary Change* 63:
670 317-324.
671 Tyler JJ, Leng MJ and Sloane HJ (2007) The effects of organic removal treatment on
672 the integrity of delta O-18 measurements from biogenic silica. *Journal of*
673 *Paleolimnology* 37: 491-497.

674 Vanniere B, Power MJ, Roberts N, Tinner W, Carrion J, Magny M, Bartlein P,
675 Colombaroli D, Daniau AL, Finsinger W, Gil-Romera G, Kaltenrieder P, Pini R,
676 Sadori L, Turner R, Valsecchi V and Vescovi E (2011) Circum-Mediterranean
677 fire activity and climate changes during the mid-Holocene environmental
678 transition (8500-2500 cal. BP). *The Holocene* 21: 53-73.
679 Weiss H, Courty M-A, Wetterstrom W, Guichard F, Senior L, Meadow R and Curnow
680 A (1993) The genesis and collapse of third millennium north Mesopotamian
681 civilization. *Science* 261: 995-1004.
682 Wick L, Lemcke G and Sturm M (2003) Evidence of Lateglacial and Holocene climatic
683 change and human impact in eastern Anatolia: high-resolution pollen, charcoal,
684 isotopic and geochemical records from the laminated sediments of Lake Van,
685 Turkey. *The Holocene* 13: 665-675.
686 Woldring H and Bottema S (2003) The vegetation history of East-Central Anatolia in
687 relation to Archaeology: the Eski Acigol pollen evidence compared with the Near
688 Eastern environment. *Palaeohistoria* 43/44: 1-34.
689 Woodbridge J and Roberts CN (2010) Linking neo- and palaeolimnology: a case study
690 using crater lake diatoms from central Turkey. *Journal of Paleolimnology* 44:
691 855-871.

692 Woodbridge J and Roberts CN (2011) Late Holocene climate of the Eastern
693 Mediterranean inferred from diatom analysis of annually-laminated lake
694 sediments. *Quaternary Science Reviews* 30: 3381-3392.
695

696 **Table 1** Sources of uncertainty associated with the correction of $\delta^{18}O_{diatom}$ data used in
697 this paper.

Source of uncertainty	**Magnitude of uncertainty**
Diatom isotope measurement analytical reproducibility (1σ)	0.3‰
Al_2O_3 measurement analytical reproducibility (1σ)	0.03%
Variance in Al_2O_3 composition of turbidites (from $\bar{x}$ of 14.56%) (1σ)	1.6%
Variance in $\delta^{18}O$ value of turbidites from $\bar{x}$ of 16.0‰ (1σ)	1.0‰

698

699

700 **Table 2** Lake isotope mass balance model summary

701

	δl (‰)		Tav (°C)	P (mm)	δp (‰)	Qi average	Qo average	Volume	P/E
	Mean	Range	Mean	Total	Weighted Mean	(m^3/month)	(m^3/month)	(m^3)	Annual average
Modern	0.59	1.06	11.7	356.2	–9.4	76328	39812	7500000	0.422
with no snow	0.71	1.05	11.7	356.2	–8.5	76328	39812	7500000	0.422
with double snow	0.50	1.06	11.7	356.2	–10.4	76328	39812	7500000	0.422
Mid Holocene i	1.06	1.10	11.7	295.2	–8.8	71991	32851	7500000	0.398
Mid Holocene ii	2.00	1.22	12.6	295.2	–8.8	70781	25635	7500000	0.391
	2.00	1.52	12.6	295.2	–8.8	70781	25635	6000000	0.391
Early Holocene	–2.81	1.19	10.7	356.2	–8.9	116438	86320	7500000	0.643
	–2.81	0.99	10.7	356.2	–8.9	116438	86320	9000000	0.643
with modern temperatures	–0.57	1.21	11.7	356.2	–8.9	90813	54422	7500000	0.502

702

703

704 **Figure captions**

705

706 **Figure 1** Location of Nar Gölü in Turkey and lakes Zeribar and Mirabad in Iran.

707

708 **Figure 2** Seasonal data from 2011-2012, showing increase in lake water $\delta^{18}O$ (A) and
709 temperature (B) between the estimated times of year of diatom growth (i) and carbonate
710 formation (ii).

711

712 **Figure 3** $\delta^{18}O_{diatom}$ and $\delta^{18}O_{carbonate}$ data plotted against depth, with the error bars on $\delta^{18}O_{diatom}$
713 representing the combined uncertainties from Table 1. There are no carbonate isotope data in
714 sections where there were gaps due to coring (shown by white boxes on the lithology plot) or
715 where there were high levels (>20%) of dolomite (explained in detail in Dean et al., 2015b).
716 Gaps in the diatom isotope data are due to gaps in coring or insufficient amounts of diatom
717 silica.

718

719 **Figure 4** (A) $\delta^{18}O_{carbonate}$ (with carbonate mineralogy data) and (B) $\delta^{18}O_{diatom}$, with (C) data
720 converted to $\delta^{18}O_{lakewater}$ assuming a temperature range of +15 to +20°C for the time of
721 carbonate precipitation and +5 to +10°C for the time of diatom growth. Some isotope data
722 plotted against depth are not shown against age due to issues with the chronology (discussed
723 in detail in Dean et al., 2015b).

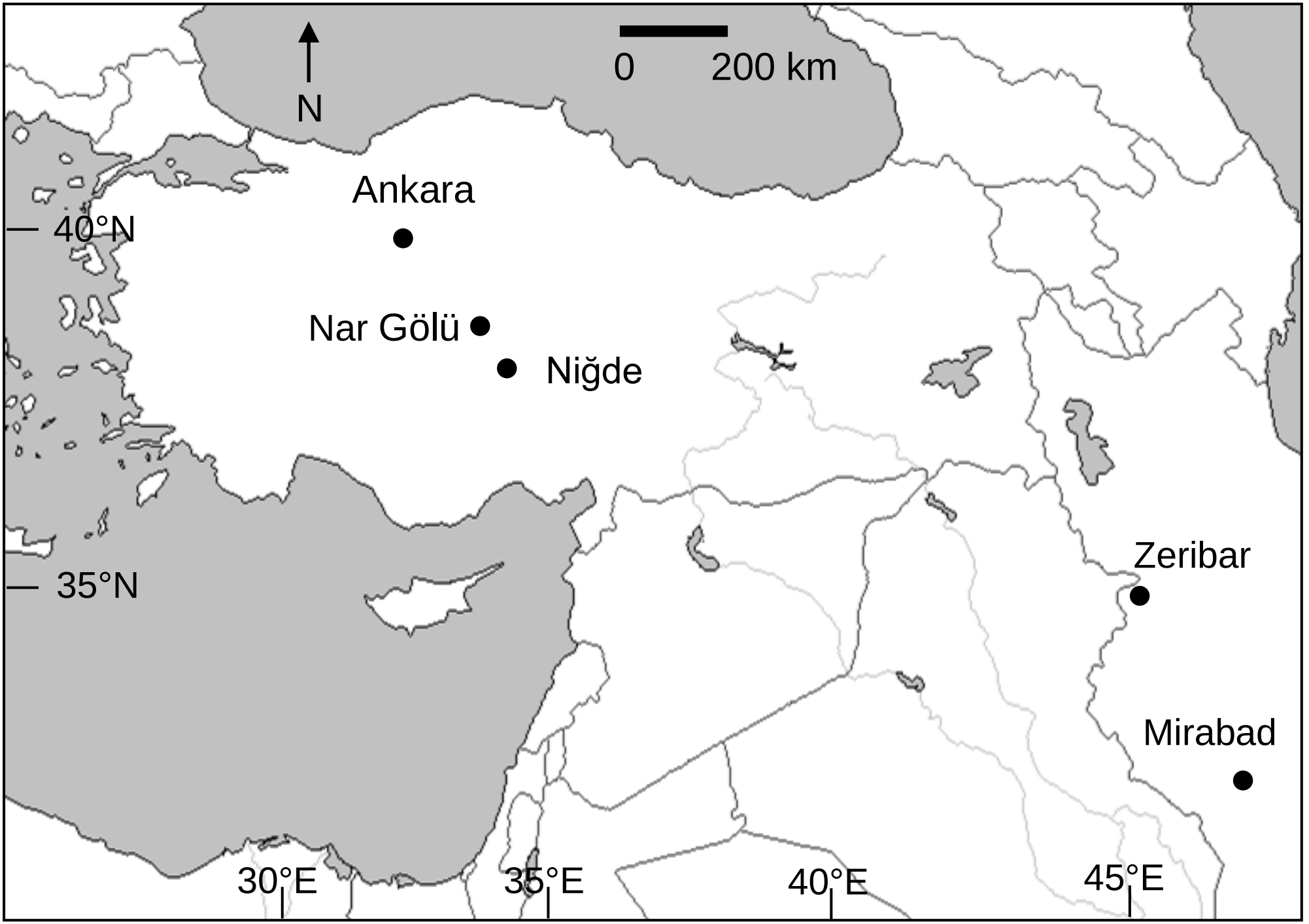
N
0
200 km
Ankara
40°N
Nar Gölü
Niğde
35°N
Zeribar
Mirabad
30°E
35°E
40°E
45°E

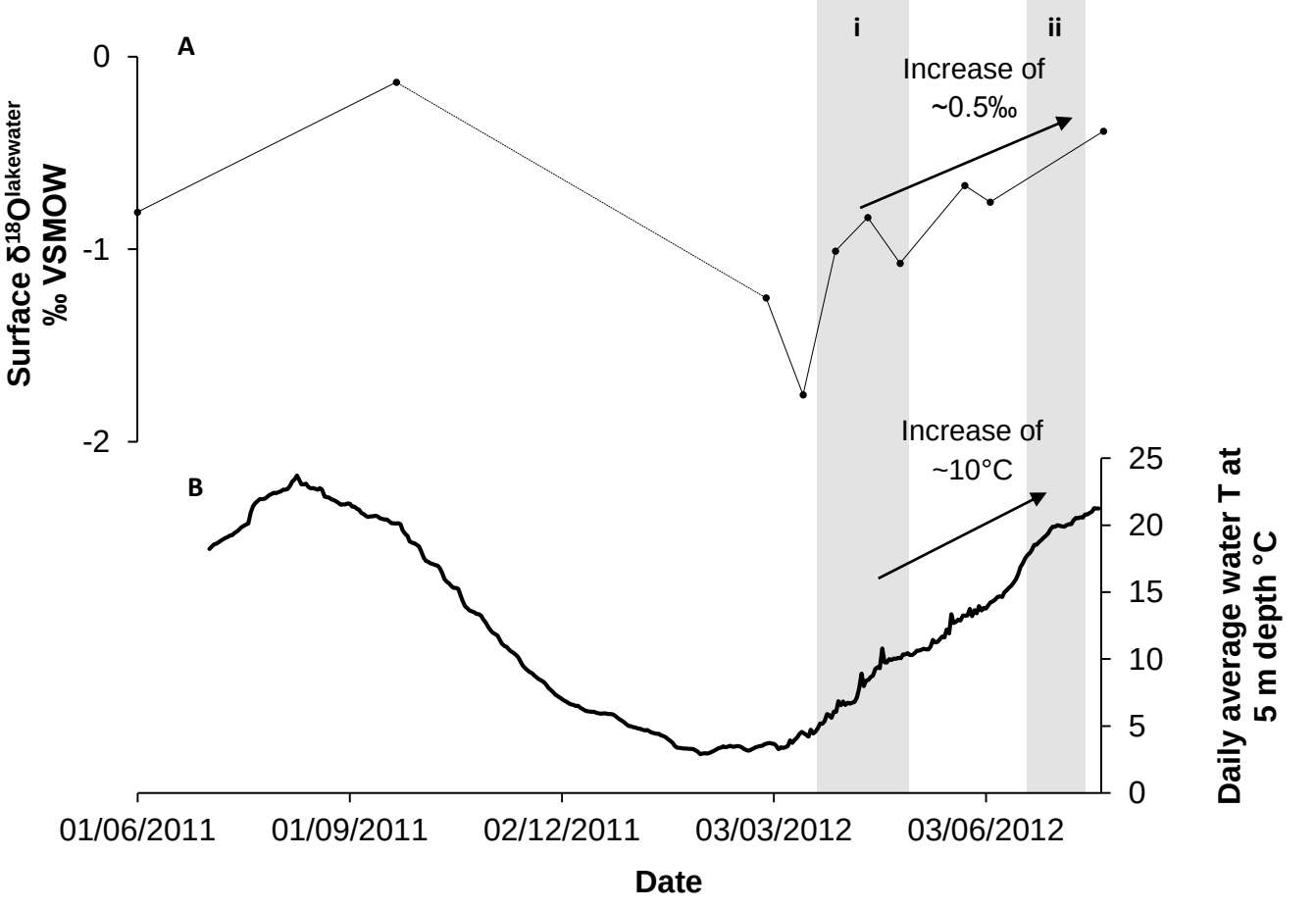
A
B
i
ii
Increase of
~0.5‰
Increase of
~10°C
0
-1
-2
Surface δ18Olakewater
‰ VSMOW
25
20
15
10
5
0
Daily average water T at
5 m depth °C
01/06/2011
01/09/2011
02/12/2011
03/03/2012
03/06/2012
Date

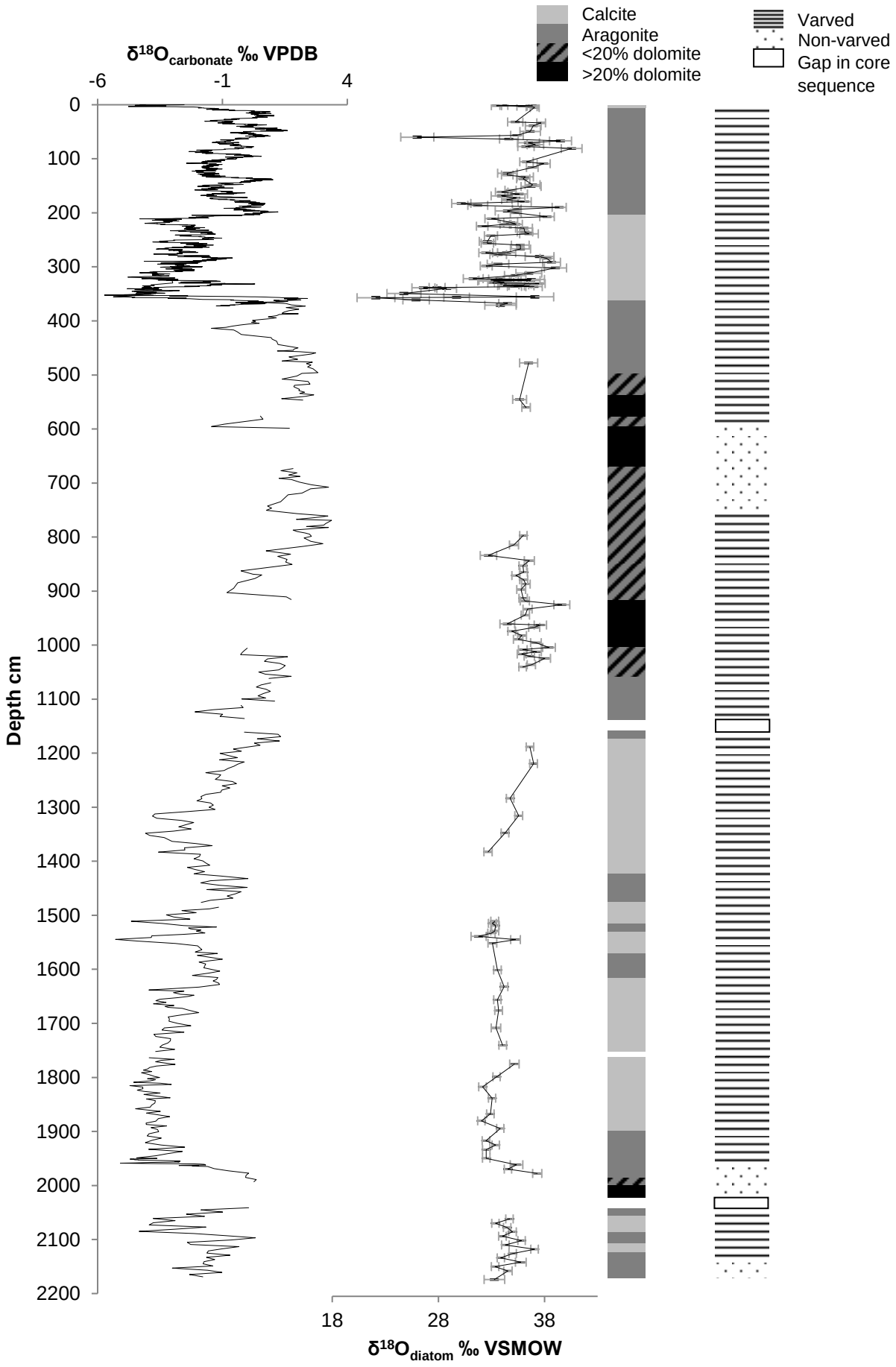
Calcite
Aragonite
<20% dolomite
>20% dolomite
Varved
Non-varved
Gap in core sequence
δ18Ocarbonate ‰ VPDB
-6
-1
4
0
100
200
300
400
500
600
700
800
900
1000
1100
1200
1300
1400
1500
1600
1700
1800
1900
2000
2100
2200
Depth cm
18
28
38
δ18Odiatom ‰ VSMOW

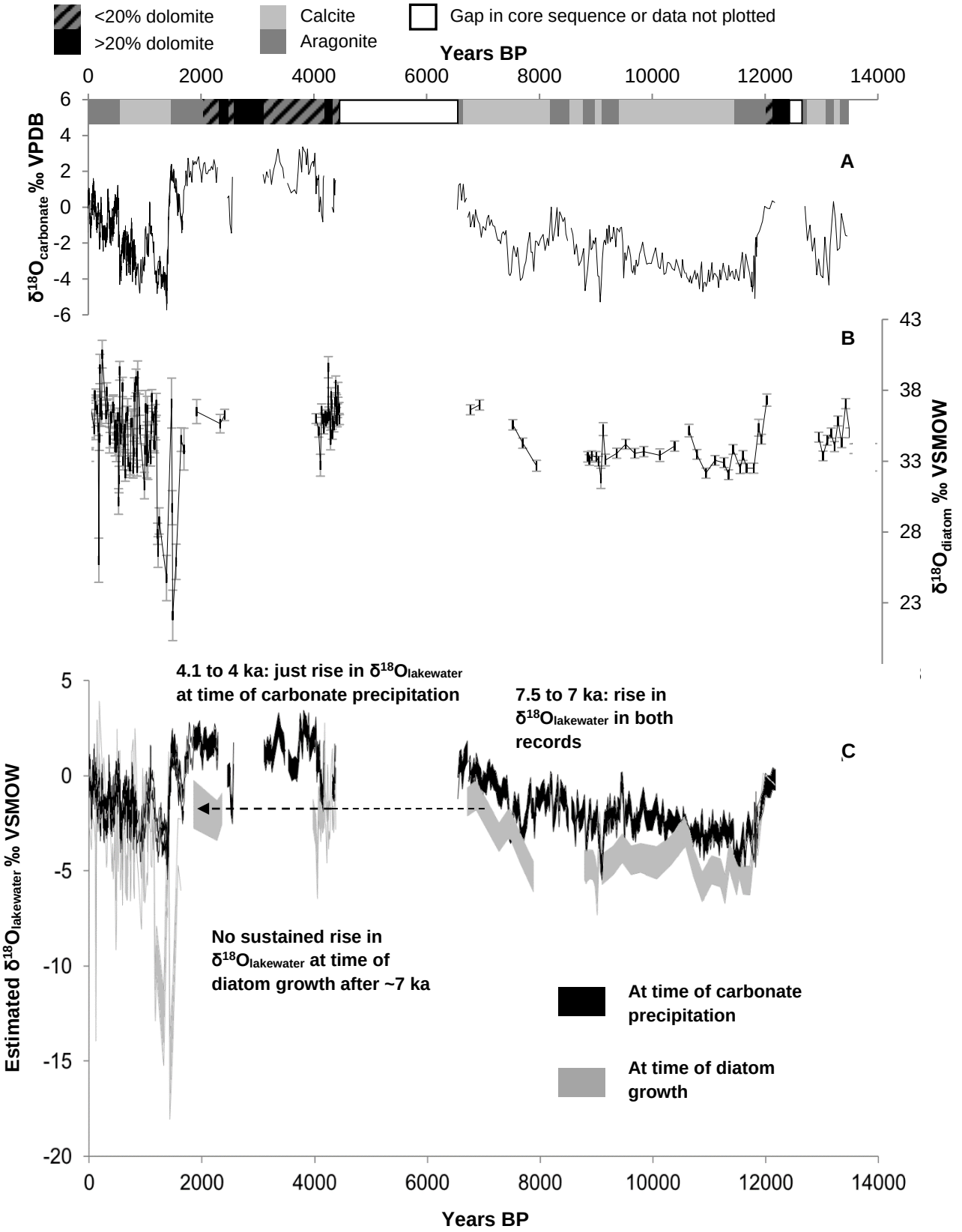
<20% dolomite
>20% dolomite
Calcite
Aragonite
Gap in core sequence or data not plotted
Years BP
0
2000
4000
6000
8000
10000
12000
14000
A
δ18Ocarbonate ‰ VPDB
6
4
2
0
-2
-4
-6
B
δ18Odiatom ‰ VSMOW
43
38
33
28
23
C
Estimated δ18Olakewater ‰ VSMOW
5
0
-5
-10
-15
-20
4.1 to 4 ka: just rise in δ18Olakewater at time of carbonate precipitation
7.5 to 7 ka: rise in δ18Olakewater in both records
No sustained rise in δ18Olakewater at time of diatom growth after ~7 ka
At time of carbonate precipitation
At time of diatom growth
Years BP

Supplementary Information for Seasonality of Holocene hydroclimate in the Eastern Mediterranean reconstructed using the oxygen isotope composition of carbonates and diatoms from Lake Nar, central Turkey

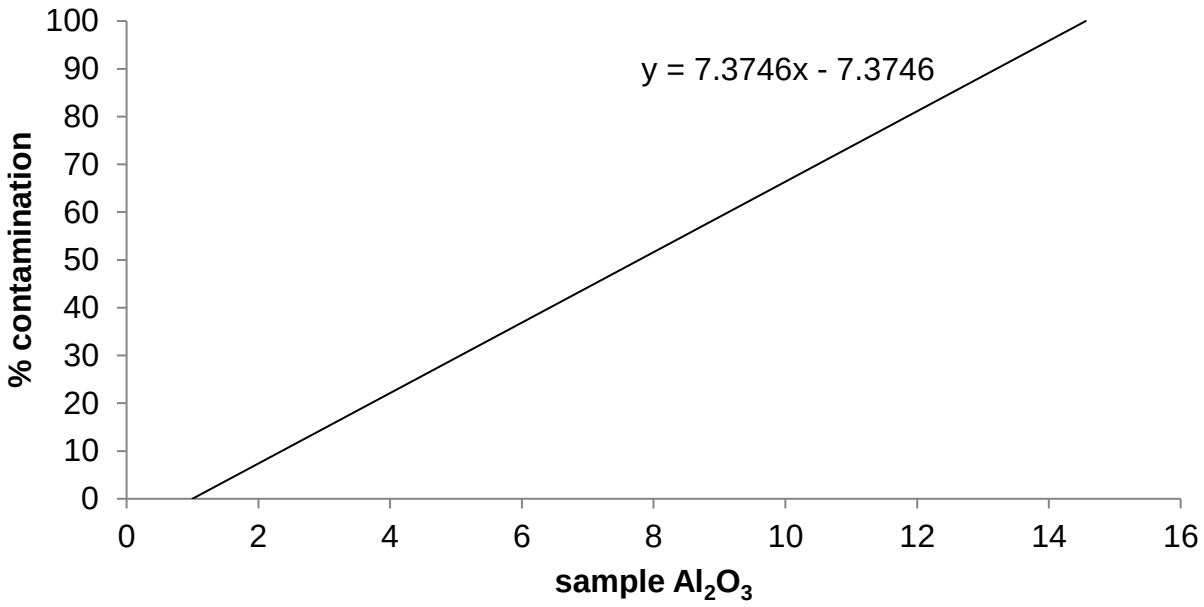

Figure SI-1 Regression line showing equation used to derive Eq. 2: a mixing line between the point when Al_2O_3 is 14.56% indicating 100% contamination and when Al_2O_3 is 1% indicating 0% contamination (i.e. 100% diatom).

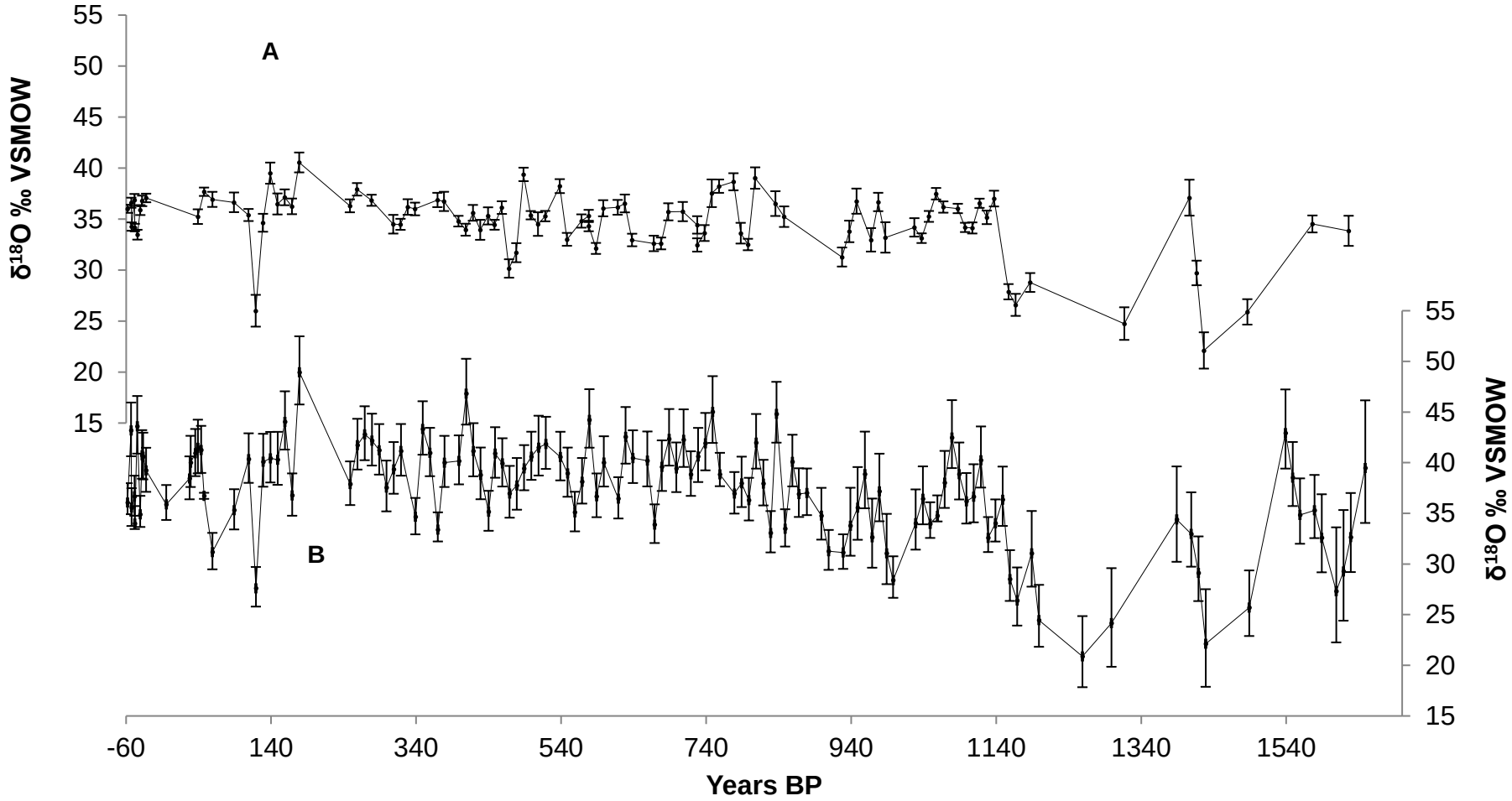

Figure SI-2 The difference between NAR01/02 diatom isotope trends in this paper (A) and as published in Dean et al. (2013) (B). Not all samples originally run and corrected in B could be included in A because many did not have sufficient material left to allow for XRF analysis. Error bars show the combined uncertainties from the factors given in Table 1.

Isotope Mass Balance Models

Theoretical model

The following is edited from Jones et al. (2016) and Jones and Imbers (2010) for the model lake used in this study.

The water mass and isotopic mass balance of a well-mixed lake is, respectively:

$$\frac{dV}{dt} = P + Qi - E - Qo \quad (1)$$

$$\frac{d}{dt}(V\delta_L) = P\delta_P + Qi\delta_P - E\delta_E - Qo\delta_L \quad (2)$$

where V is the lake volume, t, time, P, precipitation on lake surface per unit time, E is evaporation from lake surface per unit time and Q_0 and Q_i are obtained as $Q_x = S_x + G_x$, where S_0 and G_0 and S_i and G_i are the surface and groundwater outflows and inflows respectively, and are measured in the same units as P and E. δ_P, δ_E and δ_L are the isotope values, either $\delta^{18}O$ or δD, of the precipitation, evaporation and lake waters respectively.

δ_E is difficult to measure and is therefore usually calculated (e.g. Steinman et al., 2010) using equations based on the evaporation model of Craig and Gordon (1965) such that

$$\delta_E = \frac{\alpha * \delta_L - h\delta_A - \epsilon}{1 - h + 0.001\epsilon_k} \quad 3)$$

where $\alpha*$ is the equilibrium isotopic fractionation factor dependent on the temperature at the evaporating surface and

$$\frac{1}{\alpha *} = \exp(1137T_L^{-2} - 0.4256T_L^{-1} - 2.0667\times10^{-3}) \quad (4)$$

for oxygen and

$$\frac{1}{\alpha *} = \exp(24844T_L^{-2} - 76.248T_L^{-1} - 52.61\times10^{-3}) \quad (5)$$

for hydrogen. T_L is the temperature of the lake surface water in degrees Kelvin (Majoube 1971). h is the relative humidity normalised to the saturation vapour pressure at the temperature of the air

water interface and ε_k is the kinetic fraction factor; for $\delta^{18}O$ ϵ_k has been shown to approximate *14.2(1-h)* and *12.5(1-h)* for δ^2H (Gonfiantini, 1986). δ_A is the isotopic value of the air vapour over the lake and $\varepsilon = \varepsilon^* + \varepsilon_k$ where $\varepsilon^* = 1000(1-\alpha^*)$.

In the model we use an equation derived from those above to calculate the isotopic value of lake waters (δ_L) at a given time, $t+\Delta t$, based on the value of δ_L at time t, and the inputs and outputs from the lake between t and $t + \Delta t$.

The left-hand side of Eq. 2 is expanded and Eq.1 substituted into it:

$$\frac{d}{dt}(V\delta_L) = V\frac{d\delta_L}{dt} + \delta_L\frac{dV}{dt} = \delta_L(P + Qi - E - Qo) + V\frac{d\delta_L}{dt} \quad (6)$$

and then re-written, such that δ_L dependences are explicit.
δ_E is expressed as a function of δ_L such that

$$\delta_E = A\delta_L + C \quad (7)$$

where, for Equation 3

$A = \frac{\alpha*}{1-h+0.001\varepsilon_k}$ and $C = -\frac{h\delta_A+\epsilon}{1-h+0.001\varepsilon_K}$

Taking Eq. (2) and (6) and replacing δ_E using Eq. (7):

$$V\frac{d\delta_L}{dt} + \delta_L(P + Qi - E - Qo) = \delta_P(P + Qi) - E(A\delta_L + C) - Qo\delta_L \quad (8)$$

Rearranging all terms in Eq.(8) then leads to:

$$V\frac{d\delta_L}{dt} = \delta_P(P + Qi) - EC - \delta_L(P + Qi - E(1 - A)) \quad (9)$$

We define λ and β as: $\lambda = (P+Qi)\ \delta_P - EC$ and $\beta = P+Qi - E(1-A)$ such that equation (9) can be rewritten as:

$$V\frac{d\delta_L}{dt} = \lambda - \beta\delta_L \quad (10)$$

We assume that dV/dt can be adequately approximated as equal to the change of volume over 1 month and all other variables are also put into the model as rates per month.

Integrating equation (10) obtains an expression for the evolution of δ_L with time. At this stage we introduce a first approximation by assuming a constant value for V for each month; consistent with constant values of P and Qi etc. over each month. The following parameterisation for V is used:

$$\bar{V} = \frac{V_{30th}+V_0}{2} \quad (11)$$

where V_{30th} is the total volume on the last day of each month, and V_0 is the initial volume on the first day of the month.

Integration of Eq. (10) after considering the approximation in equation (11) results in:

$$\ln\left(\frac{\lambda-\beta\delta_{L0}}{\lambda-\beta\delta_L}\right) = \frac{\beta}{\bar{V}}\Delta t \quad (12)$$

Where δ_{L0} is the initial isotopic composition (i.e. at the beginning of each month) and Δt=1 for each monthly step of our model. Finally exponentials of both sides of Eq. (12) give an expression for δ_L:

$$\delta_L = \frac{1}{\beta}(\lambda - (\lambda - \beta\delta_{L0})exp(-\frac{\beta}{\bar{V}})) \quad (13)$$

Values for this model

T_L: temperature of the lake surface water

From monitoring data of Lake Nar (Jones et al., 2005, Dean et al., 2015) and other studies (Jones et al., 2016) lake surface temperatures in the model are taken as the average of mean and maximum air temperatures.

h: normalised relative humidity

Relative humidity values were calculated based on present day relationships with temperature (c.f. Jones et al., 2005) such that these values could change in time in palaeo scenarios.

These values were normalised to the conditions at the lake surface using the saturation vapour pressure of the air and surface water as defined in Steinman et al. (2010).

E: Evaporation

Evaporation is calculated based on the equation of Linacre (1992) that has been shown previously (Jones et al., 2005; Jones et al., 2007) to be a reasonable measure of evaporation and is especially useful for palaeo-contexts where instrumental measurements are non-existent.

$$E(mm/day) = [0.015 + 4 \times 10^{-4} T_a + 10^{-6} z] \times [480 (T_a + 0.006z)/ (84 - A) - 40 + 2.3 u (T_a - T_d)] \quad (14)$$

where T_a is air temperature (°C), z = altitude (m), A = latitude, T_d = dew point temperature = 0.52 $T_{a\ min}$ + 0.60 $T_{a\ max}$ – 0.009 $(T_{a\ max})^2$ – 2 °C.

δ_P: isotopic composition of precipitation

Values for the isotopic composition of rainfall at Nar came from the Online Isotopes in Precipitation Calculator (Bowen et al., 2005; Bowen, 2016).

Isotopic values of snow were based on sampling of snowfall from the catchment (Dean et al., 2013) and were fixed at –15‰ (i.e. more negative than rainfall).

Monthly values are kept as modern throughout, although the weighted annual mean values change as the amount of precipitation in a given month changes in each scenario (Table 2).

Qi: surface and groundwater inflow

The model lake has no surface inflow; this is similar to Lake Nar where there are no permanent stream inflows to the lake.

Monitoring of springs within the Nar catchment (Jones et al., 2005) has shown these to be meteoric water, such that the isotopic composition of inflowing waters to the model lake are considered to be the same as rainfall.

Values of Qi and Qo are optimised in the model to allow a stable lake with mean isotope values, and intra-annual range, similar to that of Lake Nar. In this model Qi is a function of P:E.

Qo: surface and groundwater outflow

There is no surface run off from the model lake, or from Lake Nar.

The amount of groundwater outflow is optimised for the model as described above and in the model lake is dependent on P:E, as the amount of groundwater inflow will change the flow of water through the lake, and a constant for when Qi is potentially 0 such that the lake is balanced.

Table SI-1: precipitation values (mm) used in models

Month	Modern			Mid Holocene Rainfall	Early Holocene Rainfall
	Snow	Rainfall	Total		
Jan	17.0	16.2	33.2	40.0	51.0
Feb	15.1	21.7	36.7	36.7	46.0
Mar	7.3	31.1	38.4	30.0	40.0
Apr	2.8	44.5	47.2	25.0	30.0
May		38.8	38.8	20.0	20.0
Jun		21.4	21.4	15.0	10.0
Jul		7.7	7.7	7.0	7.7
Aug		7.3	7.3	7.3	7.3
Sep		17.2	17.2	17.2	17.2
Oct		31.6	31.6	25.0	31.0
Nov	6.5	35.3	41.8	32.0	45.0
Dec	13.4	21.4	34.8	40.0	51.0

Table SI-2: temperatures for Modern and Mid Holocene I scenarios (°C)

Month	Average (Tav)	Minimum (Tmin)	Maximum (Tmax)
Jan	0.16	-4.05	5.47
Feb	1.46	-3.08	6.88
Mar	5.92	0.70	11.87
Apr	10.57	4.82	16.54
May	15.88	9.04	22.27
Jun	20.28	12.88	26.62
Jul	23.69	15.83	30.31
Aug	23.41	15.69	30.41
Sep	18.33	11.13	25.85
Oct	12.57	6.72	19.74
Nov	6.37	1.25	13.27
Dec	2.34	-1.93	7.96

Table SI-3: temperatures for Mid Holocene ii scenario (°C)

Month	Average (Tav)	Minimum (Tmin)	Maximum (Tmax)
Jan	0.16	-4.05	5.47
Feb	1.46	-3.08	6.88
Mar	5.92	0.70	11.87
Apr	10.57	4.82	16.54
May	17.00	10.00	23.00
Jun	21.50	14.00	28.50
Jul	25.00	17.00	31.50
Aug	25.50	16.50	31.00
Sep	21.50	12.00	25.85
Oct	15.00	7.00	19.74
Nov	6.37	1.25	13.27
Dec	2.34	-1.93	7.96

Table SI-4: temperatures for Early Holocene ii scenario (°C)

Month	Average (Tav)	Minimum (Tmin)	Maximum (Tmax)
Jan	0.16	0.00	5.47
Feb	1.46	0.50	6.88
Mar	5.92	0.70	11.87
Apr	10.57	4.82	16.54
May	15.00	9.04	21.00
Jun	18.00	10.00	25.00
Jul	20.00	13.00	28.00
Aug	20.00	13.00	28.00
Sep	17.00	10.00	25.00
Oct	12.57	5.00	18.00
Nov	6.37	3.00	12.00
Dec	2.34	0.00	7.00

References for supplementary information

Bowen GJ (2016) The Online Isotopes in Precipitation Calculator. Available at: http://wateriso.utah.edu/waterisotopes/pages/data_access/oipc.html Accessed: 1 August 2016.

Bowen GJ, Wassenaar LI and Hobson KA (2005) Global application of stable hydrogen and oxygen isotopes to wildlife forensics. *Oecologia* 143: 337-348.

Craig H and Gordon LI (1965) *Dueterium and oxygen-18 variation in the ocean and marine atmosphere. Stable Isotopes in Oceanography Studies and Paleotemperatures*. Pisa: Laboratory di Geologica Nucleara.

Dean JR, Eastwood WJ, Roberts CN, Jones MD, Yigitbasioglu H, Allcock SL, Woodbridge J, Metcalfe SE and Leng MJ (2015) Tracking the hydro-climatic signal from lake to sediment: a field study from central Turkey. *Journal of Hydrology* 529: 608-621.

Dean JR, Jones MD, Leng MJ, Sloane HJ, Roberts CN, Woodbridge J, Swann GEA, Metcalfe SE, Eastwood WJ and Yigitbasioglu H (2013) Palaeo-seasonality of the last two millennia reconstructed from the oxygen isotope composition of carbonates and diatom silica from Nar Gölü, central Turkey. *Quaternary Science Reviews* 66: 35-44.

Gonfiantini R (1986) Environmental isotopes in lake studies. In: Fritz, P., Fontes, J. (eds). *Handbook of Environmental Isotope Geochemistry*, vol. 3. New York: Elsevier. pp. 113-168.

Jones MD, Cuthbert MO, Leng MJ, McGowan S, Mariethoz G, Arrowsmith C, Sloane HJ, Humphrey KK and Cross I (2016) Comparisions of observed and modelled lake $\delta^{18}O$ variability. *Quaternary Science Reviews* 131: 329-340.

Jones MD and Imbers J (2010) Modelling Mediterranean lake isotope variability. *Global and Planetary Change* 71: 193-200.

Jones MD, Leng MJ, Roberts CN, Türkeş M and Moyeed R (2005) A coupled calibration and modelling approach to the understanding of dry-land lake oxygen isotope records. *Journal of Paleolimnology* 34: 391-411.

Jones MD, Roberts CN and Leng MJ (2007) Quantifying climatic change through the last glacial-interglacial transition based on lake isotope palaeohydrology from central Turkey. *Quaternary Research* 67: 463-473.

Linacre E (1992) *Climate Data and Resources: a Reference and Guide*. London: Routledge.

Majoube F (1971) Fractionnement en oxygene-18 et un deuterium entre l'eau et sa vapeur. *Journal of Chemical Physics* 187: 1423-1436.

Steinman BA, Rosenmeier MF, Abbott MB and Bain DJ (2010) The isotopic and hydrologic response of small, closed-basin lakes to climate forcing from predictive models: application to paleoclimate studies in the upper Columbia River basin. *Limnology and Oceanography* 5: 2231-2245.